Citation:

Abo, A. A[1]., Muhammad, R. J[3]., Raby, A[2]., Kyte, A[2]., Greaves, D, (2016) Analysis of high velocity free surface flow interaction with a bridge pier in a trapezoidal channel using CFD, NAFEMS International Journal of CFD Case Studies, Volume 11, pp. 5-29, May 2016

Analysis of high velocity free surface flow interaction with a bridge pier in a trapezoidal channel using CFD

Abo, A. A[1]., Greaves, D[2]., Muhammad, R. J[3]., Raby, A[2]., Kyte, A[2].

1 Marine Institute and School of Marine Science & Eng., Plymouth Univ., UK, and formerly College of Eng. University of Salahaddin -Hawler, Iraq.

2 Marine Institute and School of Marine Science & Eng., Plymouth Univ., UK.

3 Dept. of Water Resources Eng., Univ. of Duhok, Duhok-Iraq.

Abstract

This study uses the computational fluid dynamics (CFD) code ANSYS-CFX-12, to simulate 3D flow through a straight trapezoidal cross section channel containing a single bridge pier. The fluid flow condition is assumed to be steady state, isothermal and incompressible, with symmetry along the centerline of the channel, and the simulation uses the – turbulence model. The study investigates the impact of variations of aspect ratio (channel bed width/flow depth), bed and side slopes of the channel, discharge (represented by a Froude number), and the length and thickness of the bridge pier on the free surface flow profile, both along the centerline and the on the wall of the channel. The code is based on the finite volume method, and uses the volume of fluid (VOF) approach to predict the free surface flow profile.

Prediction of the free surface flow profile is essential for the design of high velocity channels. Prior prediction of flow profiles can inform and improve the design of expensive structures, such as high velocity channels and bridges, in particular the height of channel walls and bridge decks.

Firstly, the code was validated against the numerical and experimental work of Stockstill (1996) for a channel containing three piers, and found to agree well. Then, the method was applied to the design test case, and mesh convergence tests to establish the required mesh size were carried out.

The simulations were conducted in parallel over 32 cores on the Plymouth University High Performance Computer Cluster (HPCC).

Finally, a parametric study was carried out and analytical expressions derived for maximum flow depth at the centre-line and at the side wall of the channel. Useful non-dimensional

curves and equations derived from regressions of the study data are provided, which can be used as a guideline for the design of high velocity channels containing a bridge pier. For data regressions the statistical package software Statistical Product and Service Solutions (SPSS) was used.

Author keywords: High velocity channel flow, trapezoidal cross-section, bridge pier, free surface profile.

1 Introduction

The development of many cities in the Kurdistan region, and the associated municipal expansion into several floodplains, has resulted in high volumes of rainfall runoff, which frequently cause significant increases in river discharge and other high velocity channels such as sewer systems. These increased discharges may lead to floods, which may cause damage to property costing millions of dollars and also loss of life (Stockstill, 1996). To overcome this problem, the design of high velocity channels that can cope with this increased demand is imperative. An important report on high velocity channels was published by the American Society of Civil Engineering ASCE in 1951. The report includes descriptions of physical experiments undertaken by Ippen (1951), Knapp (1951), Ippen and Dawson (1951), and Rouse, Bhoota and Hsu (1951), which all discuss cells of high velocity channel design. These works provide essential descriptions of the mechanics of man-made high velocity channels, and can be used as a design guide for engineers.

Naturally occurring open channel fluid flows can be defined using the Froude number, $F_r = \frac{V^2}{\sqrt{g*D}}$, which is the ratio of inertia force to gravity force. If the Froude number is less than 1, the flow is termed subcritical and typically slow flowing, and if the Froude number is greater than 1, it is termed supercritical and is typically faster flowing and shallower than subcritical flow. The high velocity channels of interest in this work have a steep bed slope and so the velocity is high enough to achieve a Froude number greater than 1 and thus the flow is supercritical.

One dimensional (1D) flow models are often used in practical applications. Lai and Greimann (2010) mentioned examples of such models, including HEC RAS (Brunner, 2006), MIKE11 (DHI, 2002), CCHEID (WU and Vieria, 2002), and SRH-1D (Huang and Greimann, 2007). All these are also presented by Lai and Greimann (2010). Application of the 1D flow model remains particularly useful for applications with long reaches and time periods of not less than a year (Lai, 2010).

Chiu (1988) argues that the two dimensional 2D flow depth averaged model may provide the best modelling accuracy for a wide variety of natural flows. A two-dimensional numerical flow model for trapezoidal cross section high-velocity channels was developed by Stockstill (1997). This model was developed after improving the model introduced by Berger and Stockstill (1995). A trapezoidal flume was constructed by the U.S. Army Hydraulic Laboratory for model verification. The first test condition demonstrated that the model accurately solved the fluid flow and predicted correctly the waterlines through the transition where the flow accelerated from subcritical to supercritical. The experiment was then repeated by adding three piers. The model was unable to describe undular jumps which were formed in this test, but did predict choked flow upstream of the piers and compute correctly the maximum flow depth. Overall results showed that this method is useful in subcritical flow but not so efficient in supercritical flow.

Hos and Kullman (2007) investigated the ability of CFD commercial codes to solve a numerical model of a two-dimensional free surface channel flow with the existence of a bottom obstacle. ANSYS CFX was used and the simulation was built as a two phase flow model. The results show that ANSYS CFX presents the option of analyzing free surface flows without differentiating between or separately modelling subcritical, transcritical and supercritical cases.
The flow field around a vertical circular pier is categorized by several eddy systems of different sizes that develop due to the presence of the pier. Turbulent flow around vertical piers of circular cross section was modelled by Lai, Weber and Patel (2003), using the FLUENT3D numerical model. Computations were conducted by using different turbulence models and then the numerical results were compared with the experimental results. The numerical results for the bed shear stress obtained using the $k-$ turbulence model agrees reasonably with the experimental results, but with a slight variance, while the free surface height and other flow properties are predicted well. Versteeg & Malalasekera (2007) note that the $k-$ generally has poor performance when used for suddenly varying flows, such as swirling flows, rotating flows, and fully developed flows in non-circular ducts.

A correct prediction of free surface flow, both at the centerline and walls of the channel, in order to inform the wall height and bridge soffit height, in an open channel containing a bridge pier, is essential for design. The impact on the free surface flow profile, both along the centerline and the wall of the channel, of variation of the aforementioned channel parameters is investigated and the results analysed to produce design curves in this work. CFD is used for the investigation as an alternative to physical modelling as it does not require high costs and specialist facilities. A parametric study is carried out and an analytical expression derived for maximum flow depth at the centre-line and wall of the channel.

2 Numerical models

The commercial CFD code ANSYS-CFX-12 is used for the calculations presented herein and the calculations are carried out using the HPC Cluster at Plymouth University running in parallel over 32 cores.

2.1 Governing Equations

CFD code uses the finite volume method to solve the Navier-Stokes equations for fluid flow. In the case of turbulent flow simulation, flow properties such as velocity, pressure, and stresses through the flow are continually fluctuating. In tensor form the Reynolds-averaged Navier-Stokes equations RANS can be written as shown below.

The continuity equation is:

$$\frac{\partial}{\partial_{x_i}}(\rho U_i) = 0 \qquad (1)$$

where ρ = density U_i = main component of velocity, and $x =$ axis coordinate. The momentum equation is written as:

$$\frac{\partial}{\partial x_j}(\rho U_i U_j) = \frac{\partial P}{\partial x_i} + \frac{\partial}{\partial x_j}\left[\mu\left(\frac{\partial U_i}{\partial x_j} + \frac{\partial U_j}{\partial x_j}\right)\right] + \frac{\partial}{\partial x_j}(-\rho\overline{\acute{u}_i\acute{u}_j}) \qquad (2)$$

where $=$ mean pressure, u_i'= fluctuating part of the velocity, and μ = dynamic viscosity. The terms $\rho\overline{u_i'u_j'}$ in Eq. (2) are referred to as the Reynolds stresses and represent six additional unknowns in the RANS equations. In the $k-$ turbulence model, turbulence is assumed to be isotropic, so rather than model the six additional unknown Reynolds Stresses, they can be reduced to two unknowns, and the concept of turbulent viscosity used.

The VOF method of (Hirt & Nichols, 1981) is applied in order to distinguish the sharp edge between the water and the air. In this method, the interface is defined by introducing the volume fraction, α_i , where i represents the phase. The volume fraction of the i^{th} phase represents the fraction of the volume of a cell occupied by that phase.

In the VOF method, the free surface is advected by solving the transport equation for the volume fraction:

$$\frac{\partial a_w}{\partial t} + \nabla.(V.a_w) = 0 \qquad (3)$$

where α_w is the volume fraction of the water.

The volume fraction of the air phase can be found from:

$$a_a = 1 - a_w \qquad (4)$$

where α_a is the volume fraction of the air.

The solution of the above equations depends on the flow domain, which is divided into a grid composed of a large number of cells. For each cell, if occupied only by water, $\alpha_w = 1$; otherwise $= 0$. While for the cells occupied by both water and air, $0 < \alpha_w < 1$. So the flow properties in each cell can be fixed according to the local volume fraction, for example the density in each cell is:

$$\rho = a_w\rho_w + (1 - a_w) \qquad (5)$$

whereρ_w is the density of water 997 $kg.m^{-3}$, ρ_a is the density of air 1.185 $kg.m^{-3}$.

The standard $k-$ turbulence model is used for these simulations in order to achieve a reasonable balance between computational cost and accuracy. The flow is considered to be at steady state. For the spatial discretisation of advection terms, the High Resolution Scheme is selected; it uses a blend between the Upwind Differencing Scheme (1st order accurate) and the Central Difference Scheme (2nd order accurate).

2.2 Boundary conditions

Once the domain has been set up and the computational grid has been designed, the boundary and initial conditions need to be specified. For the present study, the following boundary conditions are applied.
For the inlet flow boundary condition, the average inflow velocity for a particular Froude number and flow depth is defined as shown in Table 1. The upstream pressure boundary condition can be calculated as :

$$P_{us} = (\rho_w - \rho_a) * g * a_w * (h_0 - Y) \quad (6)$$

where P_{us} is the upstream pressure, g is the acceleration due to gravity $m.\, s^{-2}$, h_0 is the upstream flow depth m, and Y is the flow depth at particular position m. Also, the inflow velocity and depth should be defined.

In fact, the flow through the high velocity channel is always supercritical due to the steep slope of the channel bed and the dominance of inertia forces in the Froude number. For this reason, the outlet boundary conditions are set up as supercritical; this type boundary condition does not require the specification of the pressure distribution, or similarly the flow depth. The outlet pressure is dependent on the flow depth approximation at the outlet, just as relative pressure of the air is required and should be set to 0 Pa (ANSYS, 2009).

The upper surface of the domain is an open boundary condition. In this kind of boundary condition, the fluid is permitted to cross the boundary surface in any direction, so the fluid might flow into or out of the domain, and a mixing of the two fluids might occur.

For the wall boundary condition the mass and momentum option should be set to 'no slip', or in other words, the mean velocity of the fluid at the wall boundary is set to zero.

$$U_{wall} = 0 \quad (7)$$

where U_{wall} is the boundary wall (wetted parameters) velocity.

To specify the wall roughness needed for turbulent flow calculations, CFX accepts only sand grain roughness, so the Manning coefficient roughness should be converted by using the equation below (Marriott & Jayaratne, 2010)

$$n = \frac{d^{1/6}}{6.7\sqrt{g}} \quad (8)$$

where n is Manning roughness coefficient $s.\, m^{-1/3}$ and d is sand grain roughness m.

Finally, it is possible to take advantage of the symmetry of the geometry along the centerline of the channel, so that only one half of the geometry is modelled. The required computation time is reduced and simulation with the appropriate finer mesh is possible; as a result accuracy may be improved for a given computational cost.

3 Code validation

The capability of CFD code to predict correctly the free surface flow profile and velocity distribution for a high velocity channel containing an obstruction was first investigated, following work by Stockstill (1996). Simulations were solved for a multi-phase, steady state, isothermal and incompressible fluid flow, with symmetry boundary conditions along the centerline of the channel, and the standard $k-$ turbulence model. First of all the values of the boundary layer thickness, y^+, defined in Equation (9), were checked, which for the $k-$ turbulent model should be $y^+ < 300$ (ANSYS, 2009).

The domain was meshed with swept hexahedral cells of 1cm maximum side length. Different refinement mesh techniques were used, namely: inflations at the wetted perimeter in order to capture required y^+ grid refinement in the vicinity of piers; in order to capture sharp changes in flow properties occurring due to the presence of the bridge pier; and increasing number of sweep division in the vertical direction to predict free surface flow correctly.

The y^+ is a non-dimensional wall distance from a wall-bounded flow, its value can be calculated as follows:

$$y^+ = \frac{u_* \delta}{\gamma} \tag{9}$$

where u_* is the friction velocity at the nearest wall, δ is the thickness of the first layer cell adjacent to the wall and γ is the local kinematic viscosity of the fluid. The friction velocity,

$$u_* = \sqrt{\frac{\tau_w}{\rho}} \tag{10}$$

where τ_w is the wall shear stress and ρ is the fluid density at the wall.

The code's ability to predict free surface flow both along the wall and the centerline of the channel, and velocity profiles at three different positions was assessed. For this purpose the experimental and computational results of Stockstill (1996) are considered.

Work was carried out numerically and experimentally by Stockstill (1996) to describe the flow in trapezoidal channels, and the same case is simulated here using CFD code. The trapezoidal cross-section channel had a bed width of $B = 0.61$ m and 1:2.25 side slopes, and contained three piers with rounded ends of length $Pl = 0.31$ m and thickness $Pt = 0.03$ m, the centerline of the pier is located at 9.3 m from the upstream boundary as shown in Figures 1 and 2. The wall roughness was 0.009, which is equivalent to 0.0454 mm grain size according to Equation 8.

The grid size is set to 0.01 m, the initial computational mesh is 3624788 vertices and 5534182 cells. Computation time approximately was 120 hours to converge solutions using the HPC cluster with 32 cores in parallel.

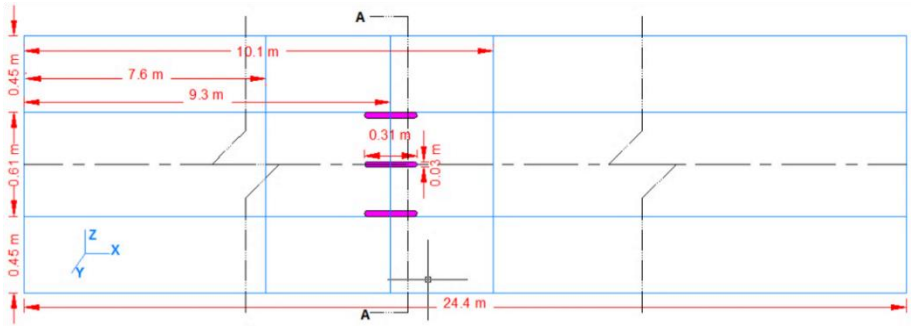

Figure 1: - Typical channel plan, Stockstill (1996).

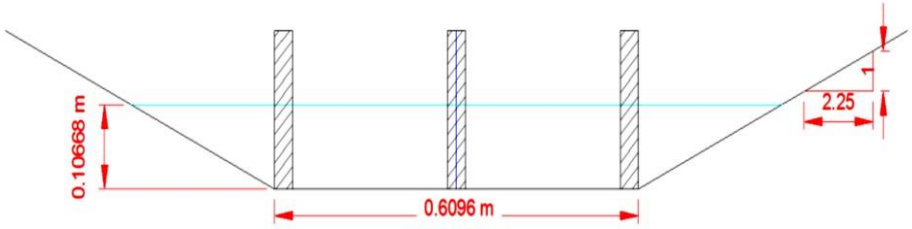

Figure 2:- Cross section A-A

The code HIVEL2D was used by Stockstill (1996) for numerical calculations. This code is based on the finite element method and uses a Petrov-Galerkin component to control numerical oscillations due to advection.

The CFD code results (labelled CFX) are plotted on the same graphs together with the experiment results (Stockstill, 1996), termed Stockstill Flume, SF, and numerical results, termed Stockstill Model, SM, in Figures 3 and 4, respectively.

It is clear from Figures 3, 4 and 5-a, b, and c, that in comparison between the CFX, SF and SM results for free surface profile both at the centerline and the wall of the channel, and the velocity distribution at three different positions – upstream, centerline, and downstream of the piers – CFX agrees better with the physical experiment results (SF) than with the previous numerical results (SM). Also, from Figures 3 and 4 it is clear that the physical principles of the hydraulics of open channels are adhered to, in that the flow depth upstream of the pier is significantly increased due to stagnation occurring at the pier, where the flow velocity drops to zero. These events can be clearly observed upstream of the pier both at the centerline and the wall of the channel. Thereafter the uniform flow is re-established, as can be seen in Figures 3 and 4.

Finally, from Figures 5-a, and c, the surface velocity distributions, both upstream and downstream of the pier at the locations along the channel length 7.6 m and 10.1 m, clearly show that the conditions are approximately uniform. In Figure 5-b, the surface velocity distribution along the cross section of the channel at distance 9.3 m shows that the flow velocity is reduced at the piers and accelerated between the piers. Considering the free surface flow profiles in Figure 3 and 4, the free surface profile fluctuates downstream of the pier suggesting that the flow has become highly turbulent in this region.

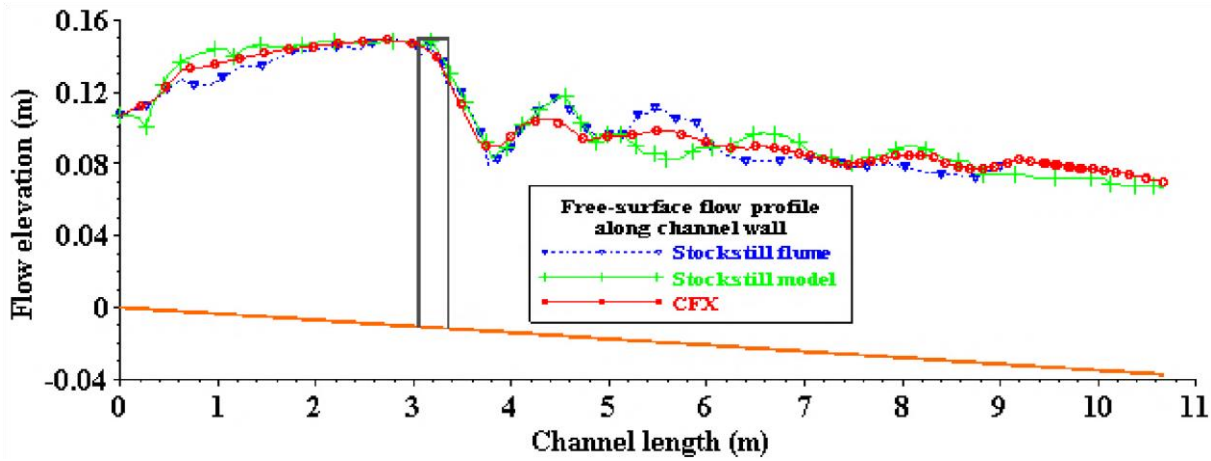

Figure 3: - CFX, SM, and SF free surface flow profile along the side wall of the channel.

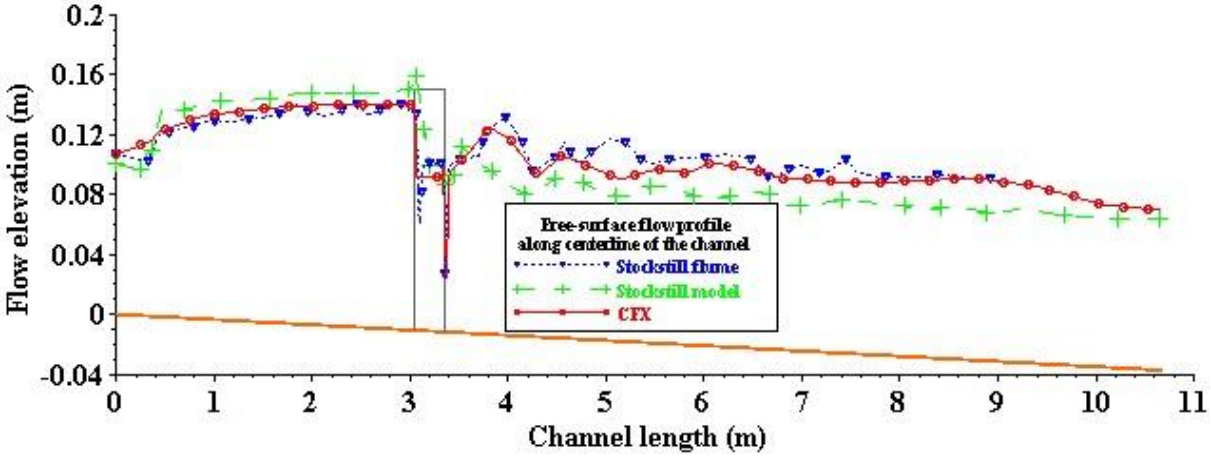

Figure 4: - CFX, SM, and SF free surface flow profile along centerline of the channel.

Figure 5-a, b, and c: - CFX, SM, and SF surface velocity profile at different positions.

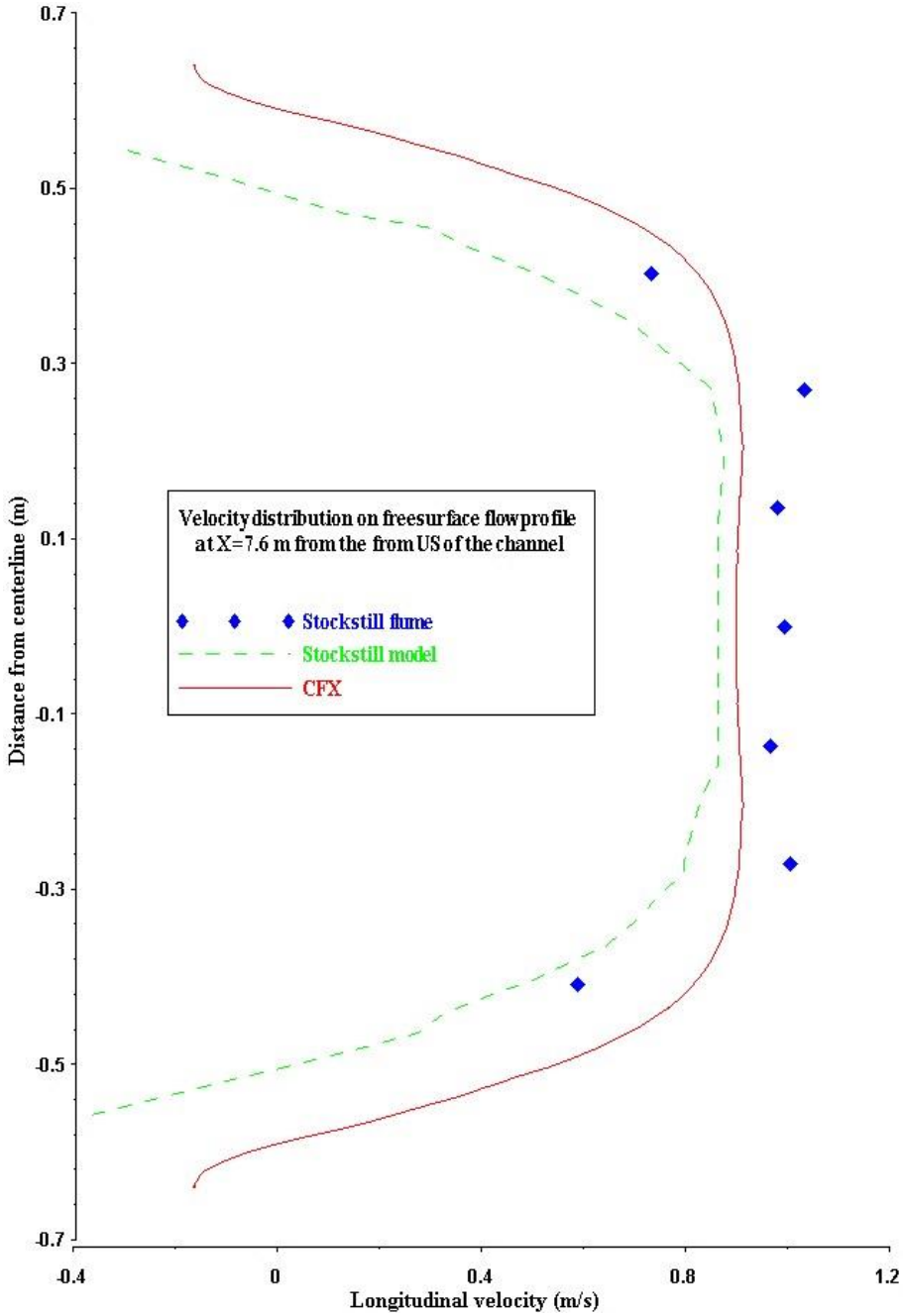

Figure 5-a: - x=7.6 m

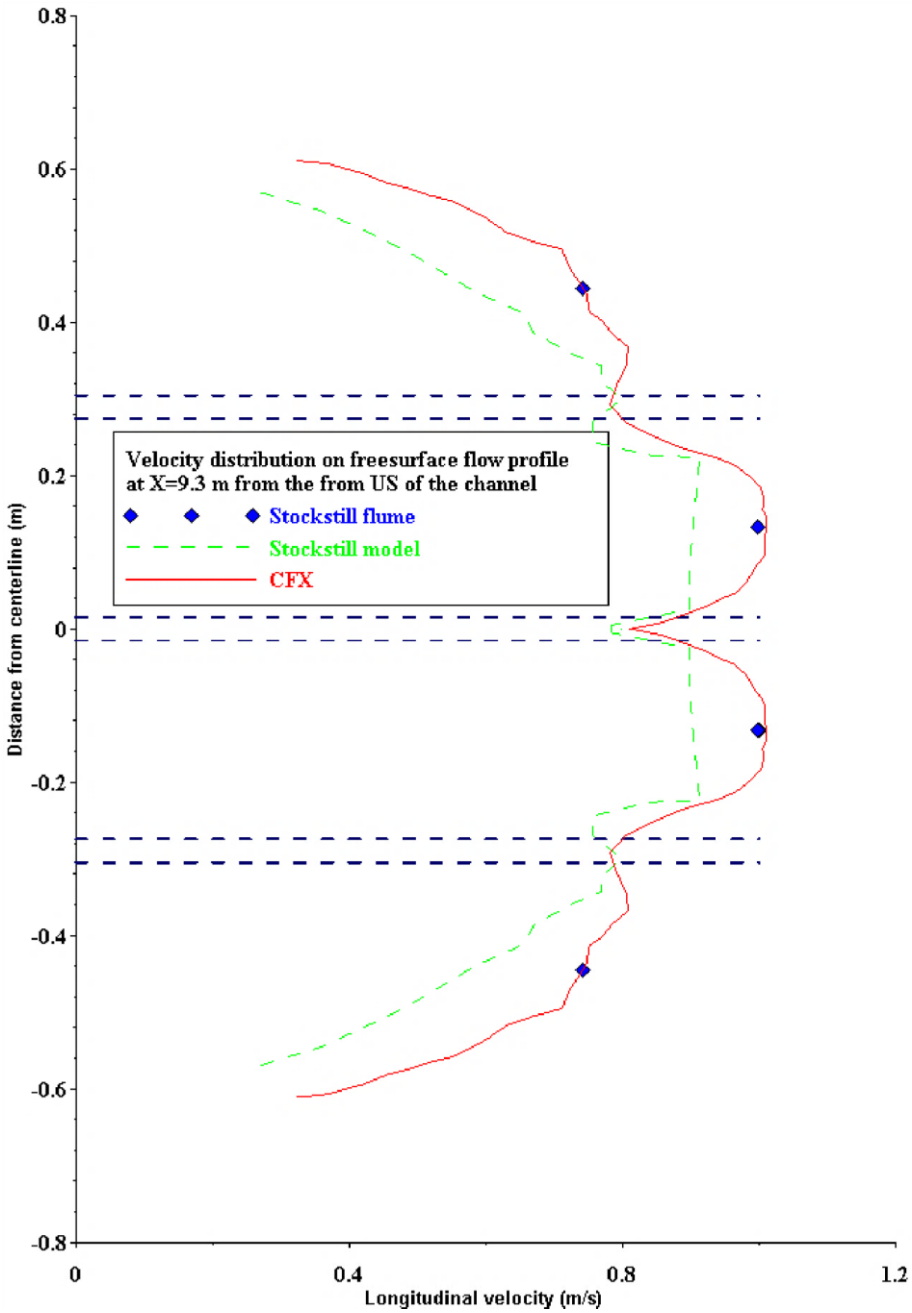
Velocity distribution on freesurface flow profile
at X=9.3 m from the from US of the channel
Stockstill flume
Stockstill model
CFX
Distance from centerline (m)
Longitudinal velocity (m/s)
0.8
0.6
0.4
0.2
0
-0.2
-0.4
-0.6
-0.8
0
0.4
0.8
1.2

Figure 5-b: - x=9.3 m

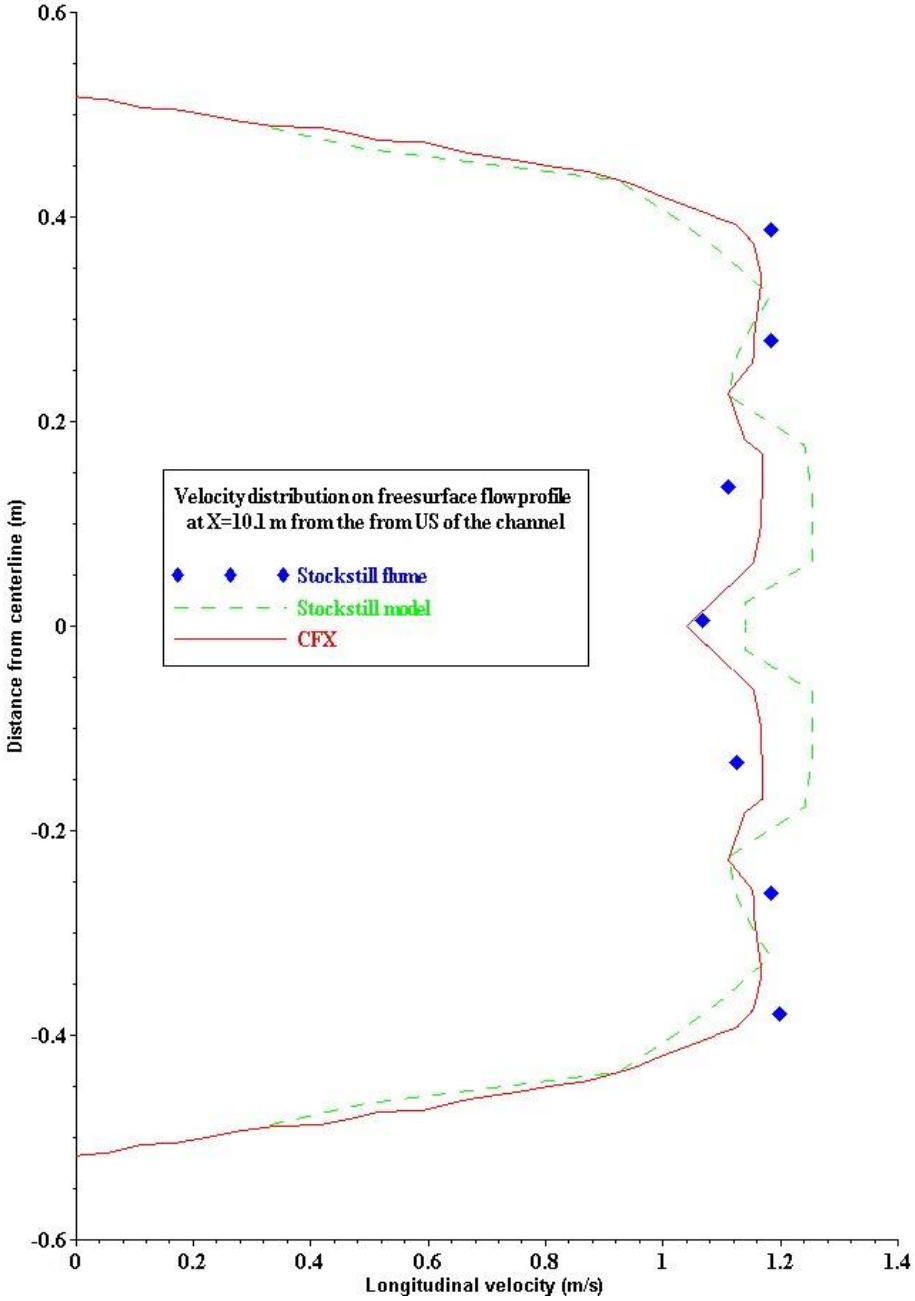

Figure 5-c: - x=10.1 m

4. Parametric study for Design

Having established that the numerical method is suitable for simulating high speed open channel flow with obstructions, the method is applied here to investigation of the parameters affecting flow conditions in order to produce design curves. A trapezoidal cross-section channel with dimensions channel bed width, height and length respectively (B*5*200) m, with three different aspect ratios (10, 8, and 6), three bed slopes (0.005, 0.006, and 0.007), three sides wall slopes (1:1, 1:1.5, and 1:2), single pier with different sizes (0.6*4, 0.6*6, 0.6*8, 0.4*6, and 0.8*6) m are simulated.

The Manning coefficient of roughness is assumed to be n = 0.012, because the channel boundary and pier are considered concrete, and according to Equation (8) equivalent to sand grain size 0.255 mm; this was kept constant for all cases. Four different discharges were considered which were represented by Froude numbers (1.25, 1.5, 1.75, and 2) using the inlet velocities depending on the above Froude numbers. And the upstream flow depth of 1.5 m was kept constant in all cases, as shown in Table 1 and Figures 6 and 7.

The flow in all cases was considered as steady-state, incompressible, isothermal, and symmetric, and the $k-$ turbulence model was used on the basis of the validation tests. The ANSYS-(with ANSYS Workbench12.0) was used as the solver and ANSYS meshing was used as the mesh generator for hexahedral cells.

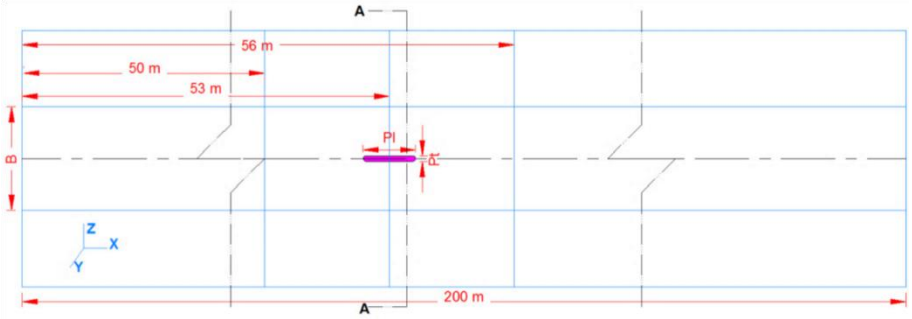

Figure 6:- Typical channel plan for single pier cases.

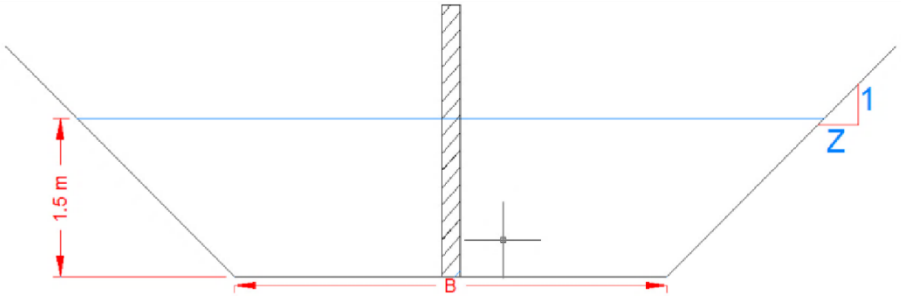

Figure 7:- Typical cross-section A-A.

The criteria considered included three different aspect ratios (6, 8, and 10) and the aim is to avoid high flow depth in open channels because such flow configurations are potentially harmful for the single bridge pier, and may contribute to its failure, as reported, for example by (Kallaka & Wang, 2011).

The three bed slopes of the channel 0.005, 0.006, and 0.007 were chosen as suitable for the topography of Kurdistan (MMSWM, 1976) and also to generate high velocity flow in the system.

The three side wall channel slopes of 1:1, 1:1.5, and 1:2 were chosen as suitable for normal construction, given the available area for the channel construction and the nature of the Kurdistan environment (MMSWM, 1976).

Finally the pier thicknesses of 0.4, 0.6, and 0.8 m, and lengths 4, 6, and 8 m were chosen to represent typical overpass or bridge structures, for example for pedestrian or vehicle use. So the test series comprised of three different aspect ratios, three channel bed and side wall

slopes, and three different pier lengths and thicknesses, each with four different Froude numbers, a total of sixty cases.

Table 1:- Details of different channel geometry and flow properties with bridge pier configurations.

Cases	Bed Width (B) m	Flow depth (h_0) m	Aspect ratio B/h_0	Bed slope	Side wall slope (z)	Froude number	Pier dimension (m)	Inflow velocity (m/s)
Impact of aspect ratio (channel width/flow depth)								
1.1-1	15	1.5	**10**	0.006	1:1.5	1.25	6*0.6	4.51
						1.5		5.412
						1.75		6.314
						2		7.22
1.1-2	12	1.5	**8**	0.006	1:1.5	1.25	6*0.6	4.46
						1.5		5.35
						1.75		6.24
						2		7.13
1.1-3	9	1.5	**6**	0.006	1:1.5	1.25	6*0.6	4.38
						1.5		5.25
						1.75		6.13
						2		7.004
Imp act of va riation o f channel bed slope								
1.2-1	12	1.5	8	**0.005**	1:1.5	1.25	6*0.6	4.46
						1.5		5.35
						1.75		6.24
						2		7.13
1.2-2	12	1.5	8	**0.006**	1:1.5	1.25	6*0.6	4.46
						1.5		5.35
						1.75		6.24
						2		7.13
1.2-3	12	1.5	8	**0.007**	1:1.5	1.25	6*0.6	4.46
						1.5		5.35
						1.75		6.24
						2		7.13
Impact of variation of slant angle (side walls slope)								
1.3-1	12	1.5	8	0.006	**1:1**	1.25	6*0.6	4.55
						1.5		5.46
						1.75		6.37
						2		7.28
1.3-2	12	1.5	8	0.006	**1:1.5**	1.25	6*0.6	4.46
						1.5		5.35

						1.75		6.24
						2		7.13
1.3-3	12	1.5	8	0.006	**1:2**	1.25	6*0.6	4.38
						1.5		5.25
						1.75		6.13
						2		7.004
Im pact of variation of transit ion length								
1.4-1	12	1.5	8	0.006	1:1.5	1.25	**4*0.6**	4.46
						1.5		5.35
						1.75		6.24
						2		7.13
1.4-2	12	1.5	8	0.006	1:1.5	1.25	**6*0.6**	4.46
						1.5		5.35
						1.75		6.24
						2		7.13
1.4-3	12	1.5	8	0.006	1:1.5	1.25	**8*0.6**	4.46
						1.5		5.35
						1.75		6.24
						2		7.13
Imp act of variation of transition thickne ss								
1.5-1	12	1.5	8	0.006	1:1.5	1.25	**6*0.4**	4.46
						1.5		5.35
						1.75		6.24
						2		7.13
1.5-2	12	1.5	8	0.006	1:1.5	1.25	**6*0.6**	4.46
						1.5		5.35
						1.75		6.24
						2		7.13
1.5-3	12	1.5	8	0.006	1:1.5	1.25	**6*0.8**	4.46
						1.5		5.35
						1.75		6.24
						2		7.13

4.1 Mesh dependency test

After confirmation of the validity of CFD code to predict free surface flow and velocity distribution profiles, and before going through the recommended cases in Table 1, the grid size mesh (GSM) convergence dependence should be checked in order to confirm that the grid selected is suitable for the test cases considered. The GSM significantly effects the accuracy of the results and with successively finer grids, greater accuracy can be obtained. Also, GSM significantly affects the computational expense, so a balance should be struck between accuracy and computation time in order to achieve a solution of sufficient accuracy

at reasonable computational cost. In order to assess grid convergence for this case, three cases are simulated with the same geometry, boundary conditions, and different minimum mesh side length of 1.2, 1, and 0.8 m respectively.

The GSM with 1.2 m is generated for the geometry in Figure 6. The inflation technique is applied to the walls with first layer thickness of 0.00072 m to predict required y^+ correctly, and the CFX body fitting mesh technique is applied around the piers with minimum side length of mesh 0.24 m to capture small scale flow properties in the wake of the pier. Also the mesh in the vertical direction of flow is refined by using a sweep method to predict the correct free surface flow profile. The total number of cells and vertices are 975100 and 1012626 respectively. For the cases of GSM with element size 1 and 0.8 m the same procedures are applied, except the first layer thickness is 0.0006 and 0.00048 m, and for the body fitting technique, the mesh size used is 0.2 and 0.16 m respectively. The total number of cells and vertices for mesh size 1 m are1975000 and 2032827, while for mesh size 0.8 m these are 2508800 and 2576106 respectively; see Figures 8 and 9 which represent mesh generations with mesh size 1 m.

HPCC with 32 cores was used for computations and all the residual targets were set at 10^{-9}. The total computational time required for cases with 1.2, 1, and 0.8 m was 48, 76 and 112 hours respectively. The average values of y^+ are 163, 38, 37 respectively for GSM 1.2, 1, and 0.8 m. The results outlined from the three cases were compared together: the free surface elevation at the centerline and the side wall of the channel, and velocity distributions at three different positions along the channel length: 50 m, 53 m, and 56 m. These are plotted together in Figures 8, 9, 10 11, and 12-a, b, and c.

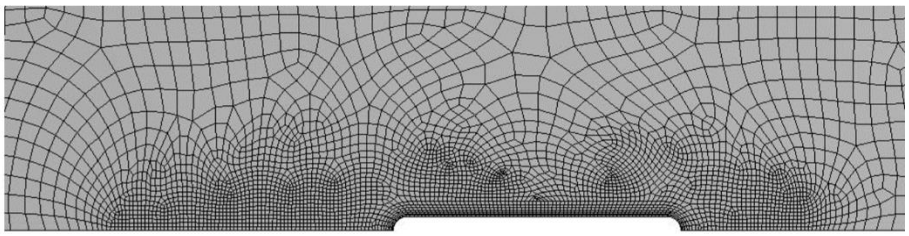

Figure 8:- Mesh refinement surrounding the pier.

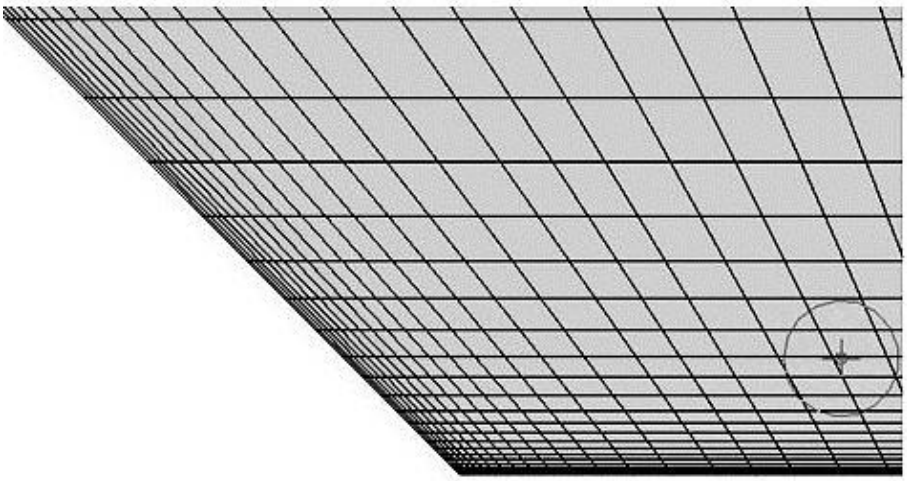

Figure 9:- Inflation layers at the channel side wall and bed.

4.1.1 Free surface flow along the centerline of the channel

Comparison of the free surface height prediction along the centerline of the channel between three different GSM (0.8, 1, and 1.2 m) shows that there is a visible difference between GSM 0.8 and 1.2 m in the latter part of the channel, see Figure 10. The reason is that the flow upstream of the pier is uniform and is accelerated due to the contraction imposed by the existence of the bridge pier; the flow is changed to non-uniform and the flow velocity again is decelerated due to expansions in cross section at the end of the pier. These changes may happen suddenly (Stockstill, 1996) and so the flow characteristics change sharply, and finer GSM be required.
The comparison between GSM 0.8 and 1 m shows that there is only slight variation between the two cases, see Figure 10.

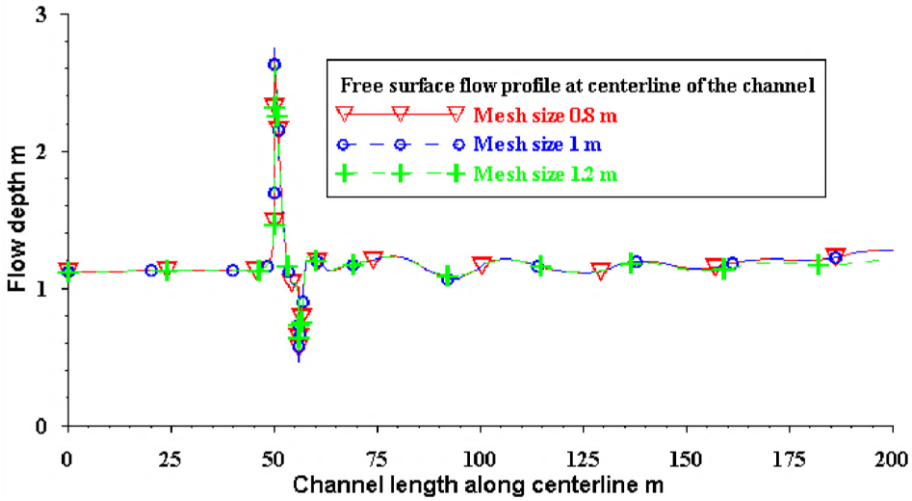

Figure 10:- Free surface flow profile along the centerline of the channel for different GSM.

4.1.2 Free surface flow along the wall of the channel

The comparisons of free surface height along the side wall of the channel between three different GSM (0.8, 1, and 1.2 m) shows that there are significant variations between two cases, GSM 0.8 and 1.2 m; see Figure 11, and much less variation between GSM 0.8 and 1.0 m.

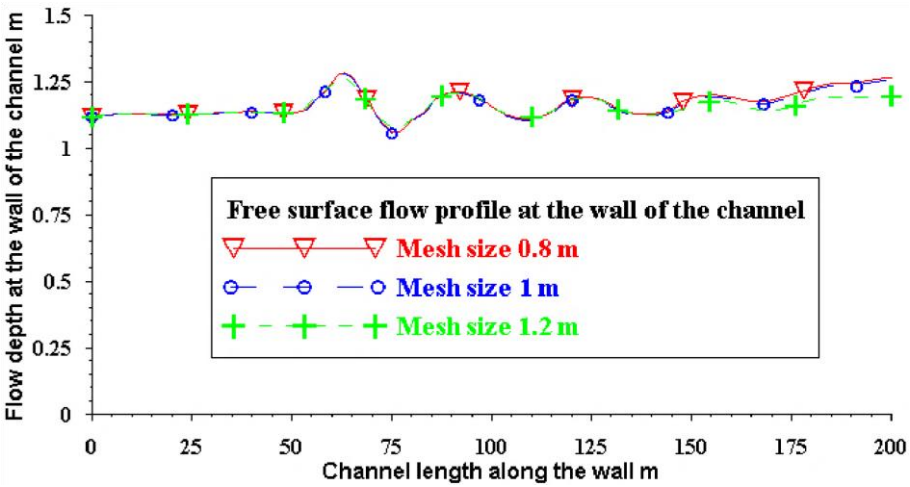

Figure 11:- Free surface flow profile along the wall of the channel for different GSM.

4.1.3 Vertical velocity profiles at different positions along the channel length

The vertical velocity profile at different positions along the channel length (50, 53, 56 m) and for different GSM (0.8, 1, and 1.2 m) are compared; see Figures 12-a, b, and c. The results show negligible variation in velocity distributions between different mesh size cases.
The results clearly demonstrate grid convergence, and now, with more confidence it can be considered that the simulation for GSM with 1 m is sufficiently converged, and the GSM 1m is therefore used for the remaining simulations.

Figure 12-a, b, and c: - Vertical velocity profile for different GSM at different positions

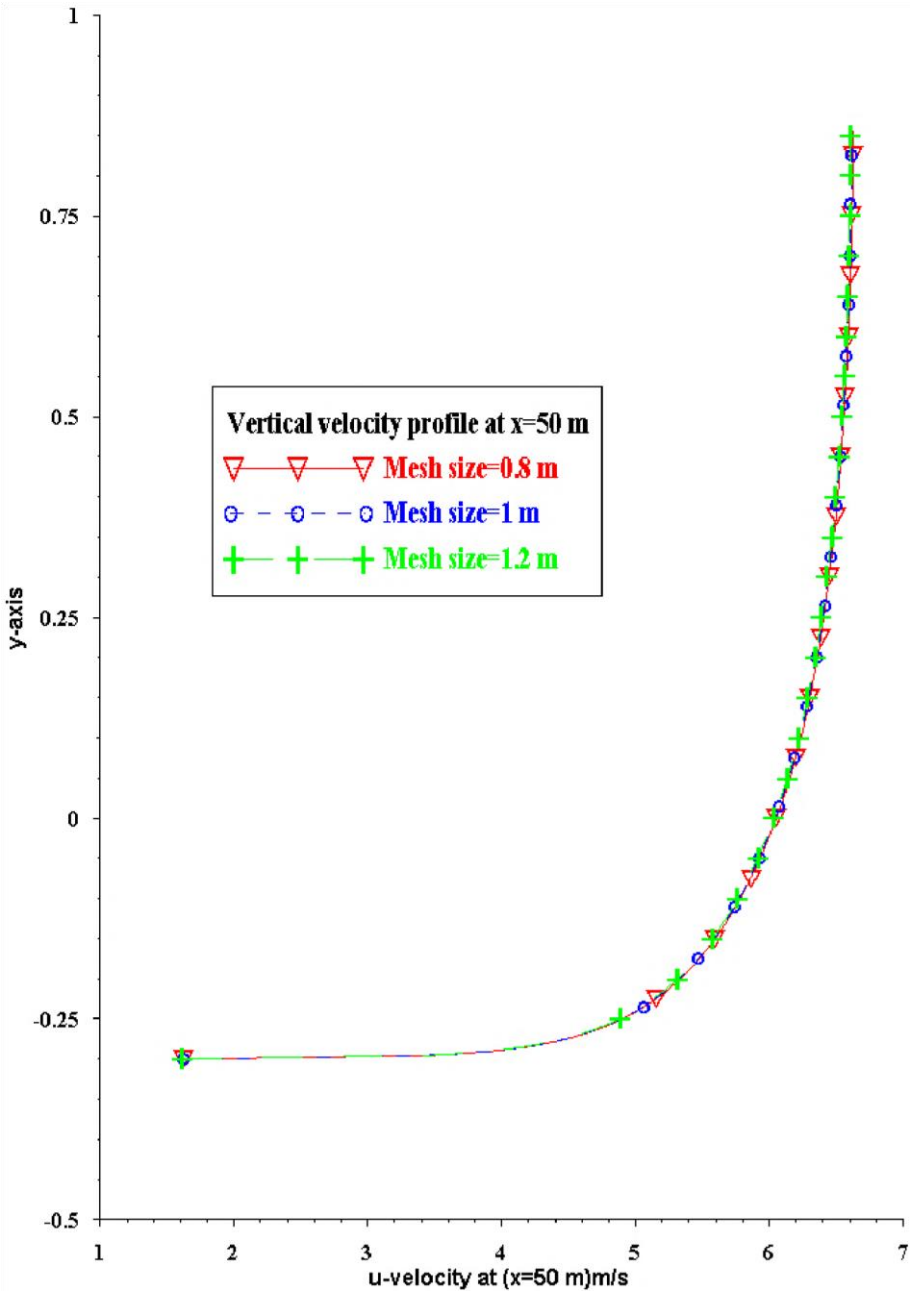

Figure 12-a:- Vertical velocity profile at the centreline at *x* = 50 m for different GSM.

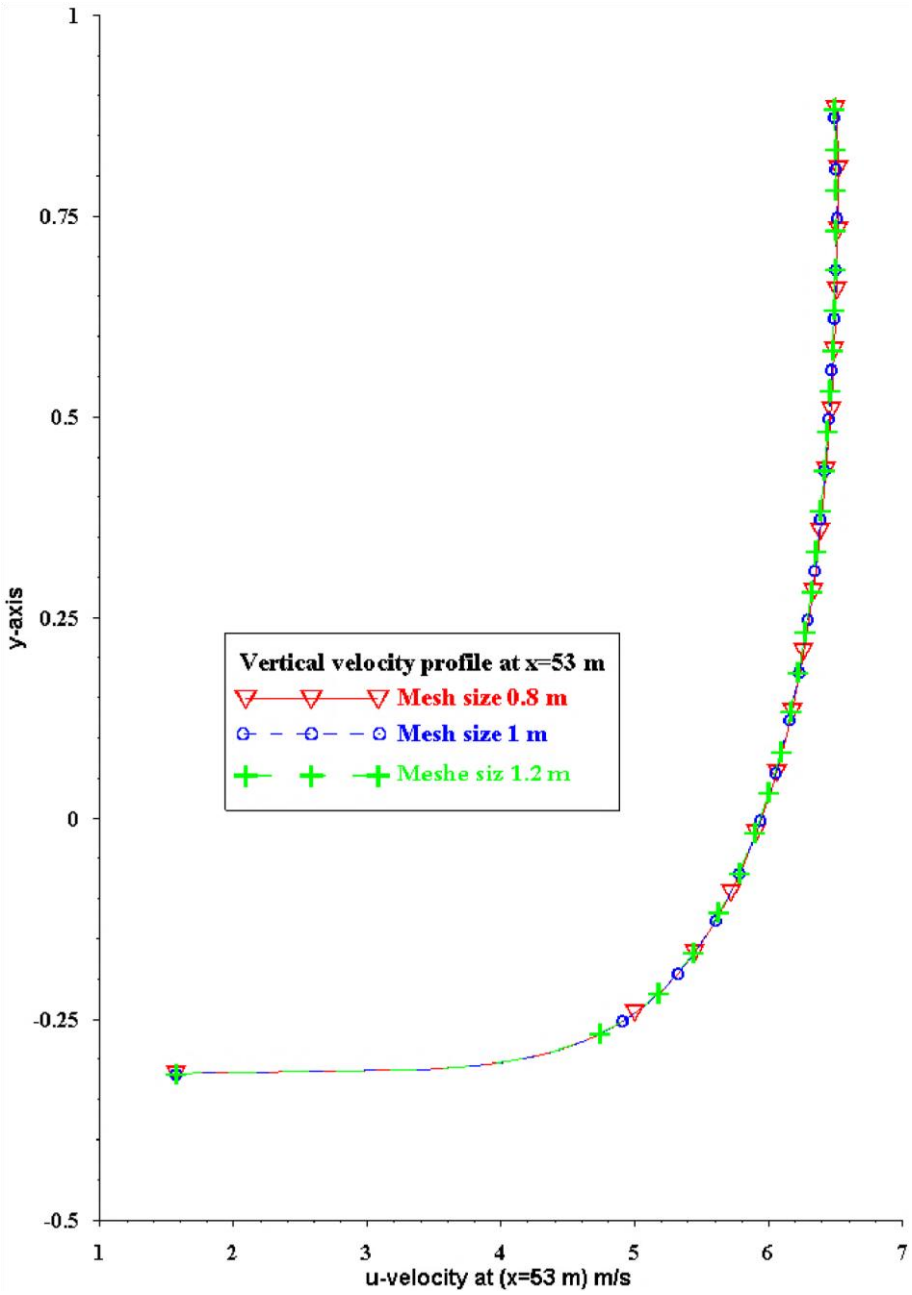

Figure 12-b:- Vertical velocity profile at the centreline at *x* = 53 m for different GSM.

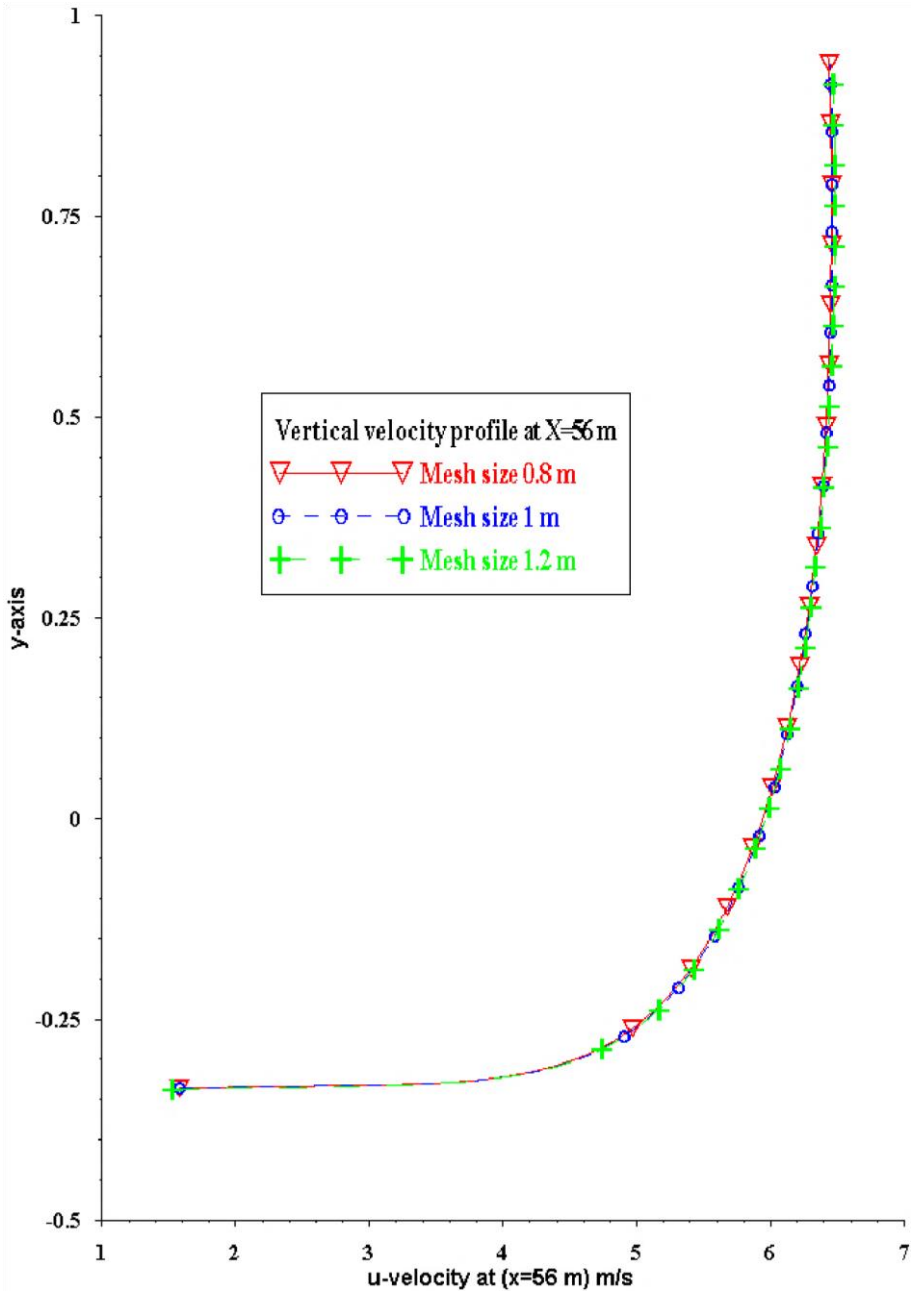

Figure 12-c:- Vertical velocity-u profile at the centreline at x = 56 m for different GSM.

4.2 Study of the impact of parameter variations on the free surface flow

The impact of variations in aspect ratio, bed and side walls slope, Froude number, pier thickness and length on the maximum flow depths along both the centerline and the wall of the channel are investigated.

4.2.1 Impact of parameter variations on the maximum flow depth along the centreline of the channel

The maximum flow depth along the centerline of the channel was not affected by variations in either aspect ratio or pier length; see Figures 13 and 16. However, the pier spacing does not

change in these cases and this is likely to have more influence on the flow depth then pier length.

The impact of variations in channel bed slope is clear in the prediction of maximum flow depth along the centreline of the channel. The maximum flow depth is inversely proportional to the bed slope; the reason being that any increase in bed slope leads to the flow velocity being increased due to gravity (French, 1985). As a result the flow discharge is accelerated as well, and the flow depth decreased; see Figure 14. The maximum flow depth is directly proportional to the side walls slope, the reason for this is that flow depth at the wall of the channel is mainly a function of wall roughness, and any increase in a side wall slope leads to increase in flow area; as a result the action of the wall roughness is decreased. See Figure 15.

Finally, the flow depth is directly proportional to pier thickness. Simply, any increase in pier thickness leads to a reduction in flow velocity, as the blockage of the channelis increased, see Figure 17.

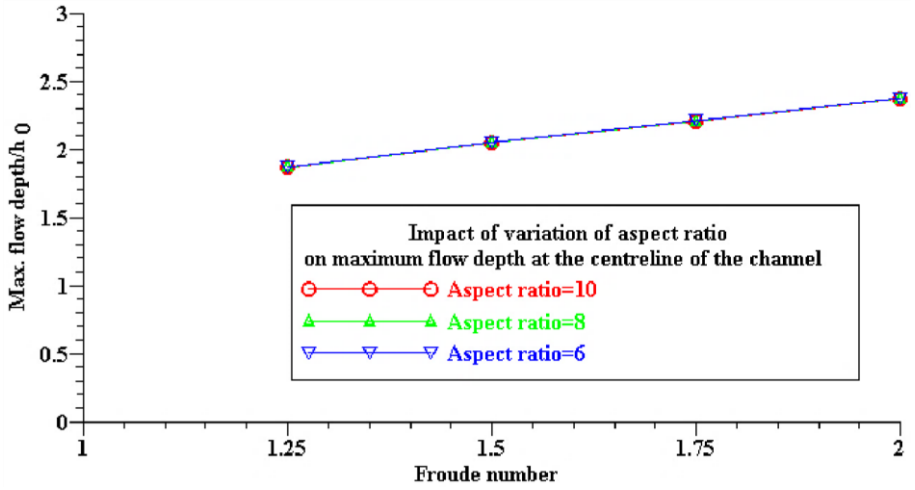

Figure 13:- Ratio of maximum flow depth to inflow depth versus Froude number along the centerline of the channel for different aspect ratios.

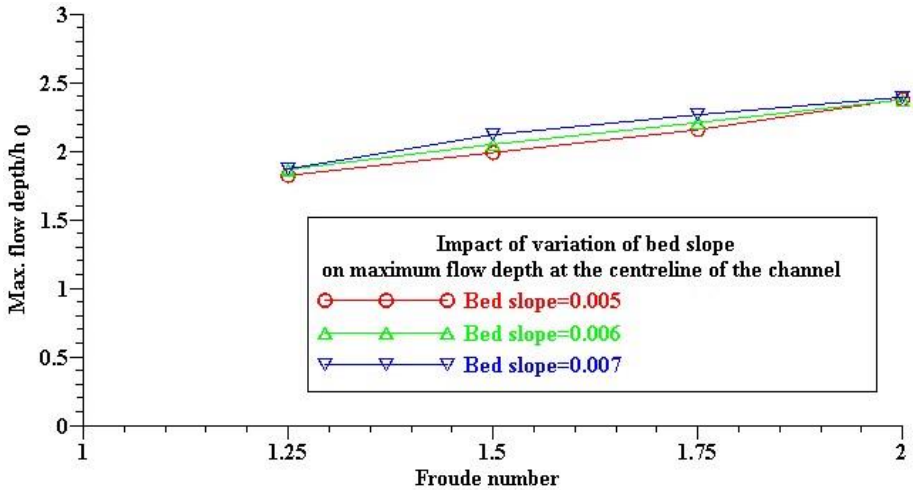

Figure 14:- Ratio of maximum flow depth to inflow depth versus Froude number along the centerline of the channel for different bed slopes.

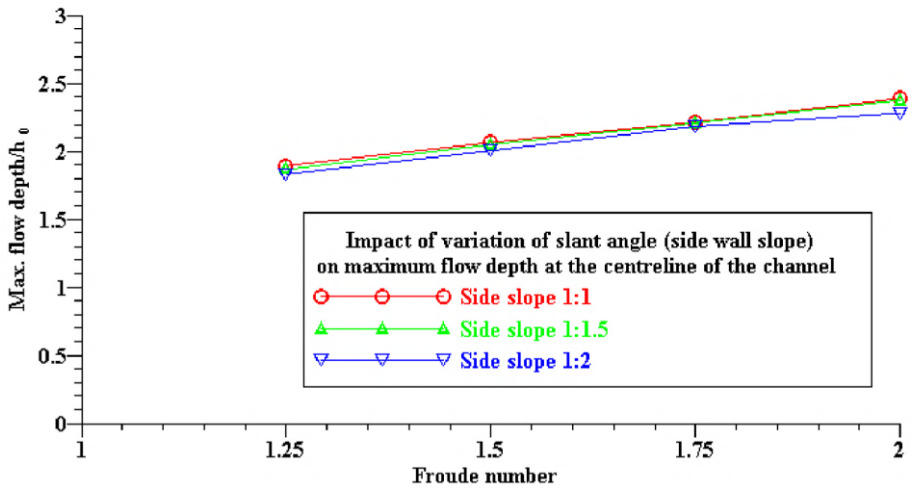

Figure 15: - Ratio of maximum flow depth to inflow depth versus Froude number along the centerline of the channel for different sidewall slopes.

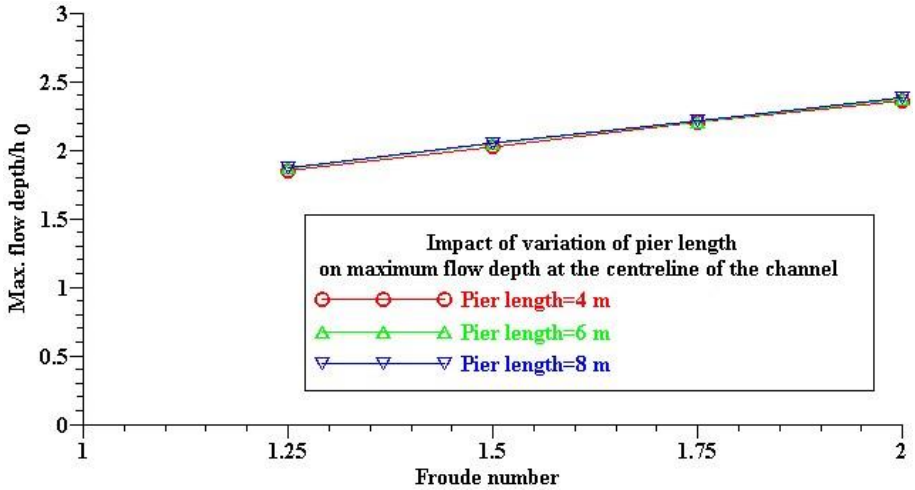

Figure 16: - Ratio of maximum flow depth to inflow depth versus Froude number along the centerline of the channel for different pier lengths.

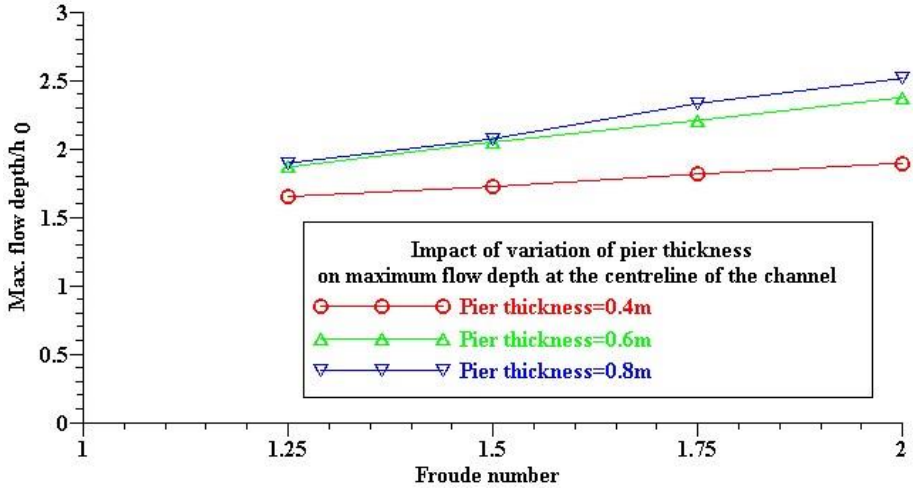

Figure 17: - Ratio of maximum flow depth to inflow depth versus Froude number along the centerline of the channel for different pier thicknesses.

4.2.2 Impact of parameter variations on the maximum flow depth along the wall of the channel

The maximum flow depth along the wall of the channel is dependent on wall roughness and the cross sectional area of the flow, as opposed to the maximum flow depth along the centreline of the channel, which depends on the velocity upstream of the pier. As observed in Figures 18, 19, 20, 21, and 22, the maximum flow depth along the wall of the channel in general increased with any increase in the discharge as well.

It can be noted from Figure 18 that the maximum flow depth along the wall of the channel increases with any decrease in aspect ratio. The reason is that the effect of wall roughness increases with any reduction in the cross-section area of the flow, and as a result the head loss increases. Also, the results show that the aspect ratio extensively affects the maximum flow depth along the wall of the channel.

From Figure 19 it can be observed that the maximum flow depth along the wall of the channel increases with any decrease in bed slope. The reason is that the flow of the steeper channel has sufficient flow velocity to pass water easily without any extra flow confluence, while this efficiency might be decreased when the channel has a less steep bed slope. Also, the results show that the bed slope of the channel has comprehensively affected the flow depth along the wall of the channel.

Any increasing of the side wall slope of the channel leads to an increase in the flow cross sectional area. As mentioned previously the effect of the wall roughness decreases with any increase in flow area. On this basis the maximum flow depth along the wall is increased with any decrease in the side wall slope of the channel; see Figure 20. Also, the results show that the side wall slope of the channel significantly affects the flow depth along the wall of the channel.

Simply put, from the results investigated in Figure 21, it can be clearly seen that the maximum flow depth along the wall of the channel is directly proportional to the pier length. The reason is that the constriction length is dependent on the pier length; as a result the flow with longer constriction should cause a greater confluence and so the maximum flow depth will increase as well. The results also show that pier length affects the maximum flow depth along the wall of the channel.

Finally, any increase in pier thickness resulted in a decrease in the cross sectional area of the channel flow. As mentioned before, any decrease in cross sectional area of the flow results in increased blockage and choking of the flow. As a result, the maximum flow depth is increased. In the absence of any other difference in channel geometry, the flow area in the contraction area decreases with any increase in pier thickness, so the maximum flow depths at the wall of the channel are increased with any increase in pier thickness; see Figure 22.

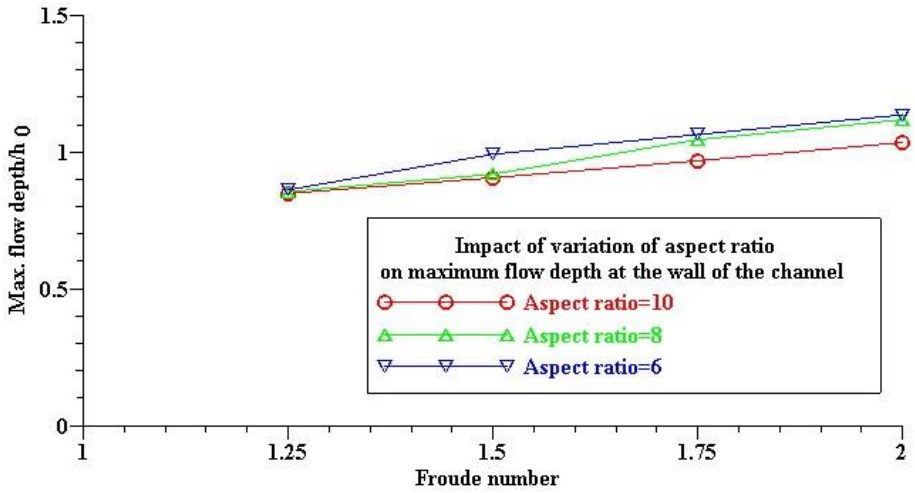

Figure 18:- Ratio of maximum flow depth to inflow depth versus Froude number along the wall of the channel for different aspect ratios.

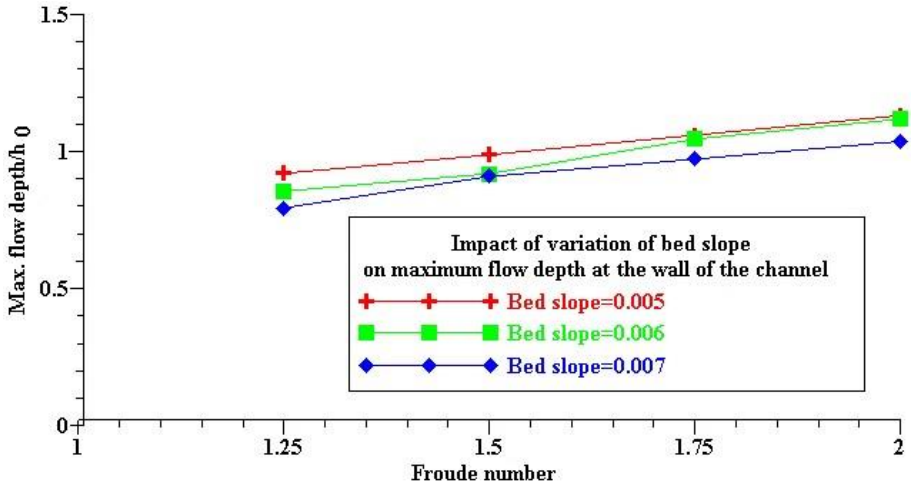

Figure 19:- ratio of maximum flow depth to inflow depth versus Froude number along the wall of the channel for different bed slope.

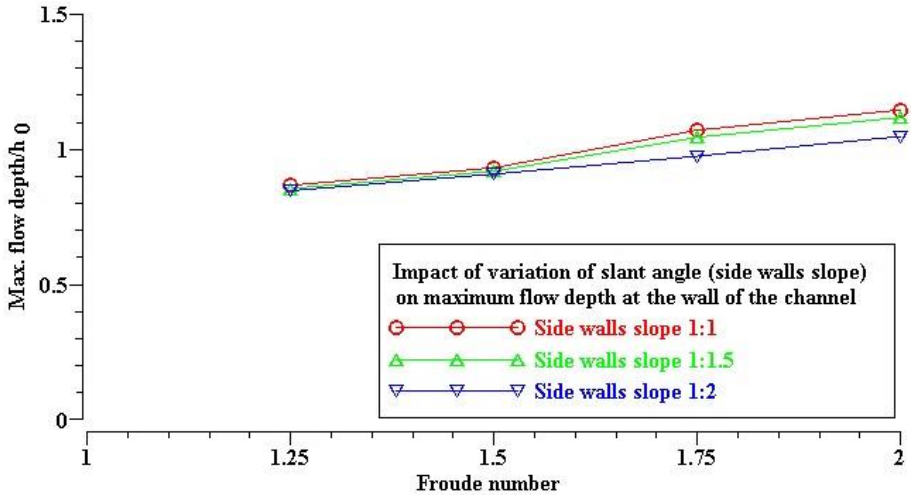

Figure 20:- Ratio of maximum flow depth to inflow depth versus Froude number along the wall of the channel for different aspect ratios.

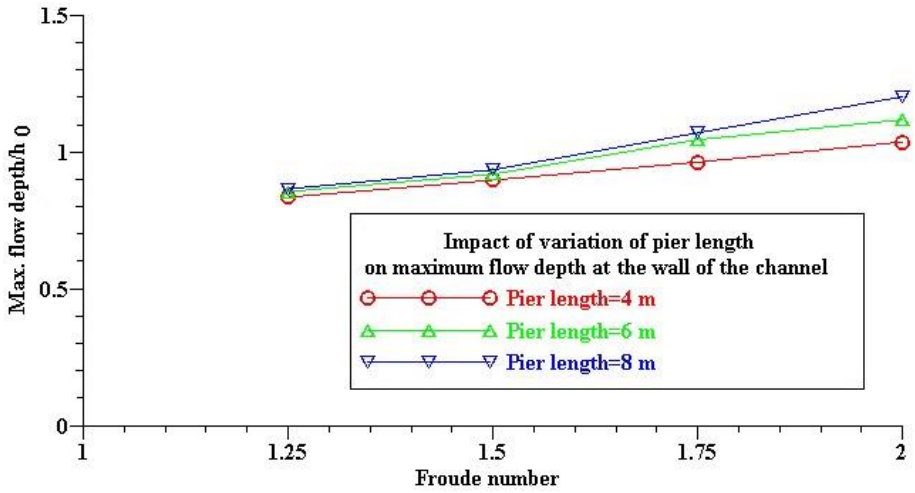

Figure 21:- Ratio of maximum flow depth to inflow depth versus Froude number along the wall of the channel for different pier lengths.

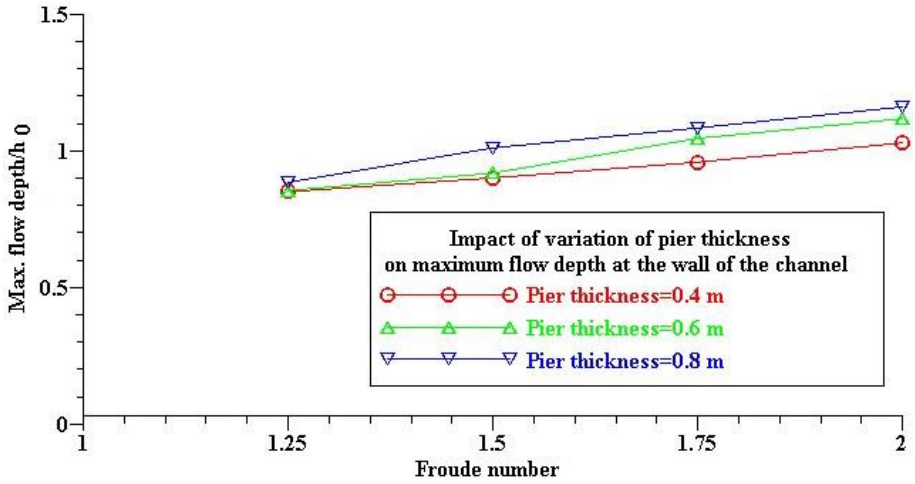

Figure 22:- Ratio of maximum flow depth to inflow depth versus Froude number along the wall of the channel for different pier thicknesses.

4.3 Data regressions

The value of maximum flow depth, both along the centerline and the wall of the channel, was assumed to be a function of factors as follows:

$$\emptyset\left(\frac{B}{h_0}, S, Z, F_r, \frac{P_l}{h_0}, \frac{P_{th}}{h_0}\right) \qquad (11)$$

Mathematically when the dependent variable is function of more than one independent variable, equation 11 can mathematically be re-arranged as follows:

$$\emptyset = a * \left(\frac{B}{h_0}\right)^b * (S)^c * (Z)^d * (F_r)^e * \left(\frac{P_l}{h_0}\right)^f * \left(\frac{P_{th}}{h_0}\right)^g \qquad (12)$$

where $\emptyset$ may be any dependent variable, B is channel bed width, h_0 is inflow depth, S is the bed slope of the channel, Z is the side wall slope of the channel, F_r is the Froude number, P_l is pier length, P_{th} is pier thickness, v is mean velocity flow, g is acceleration due to gravity, and D is hydraulic depth of the flow. For a trapezoidal cross-section channel, D can be computed by:

$$D = \frac{A}{T} \tag{13}$$

where A is the cross-section area of the flow, and T is the width of the upper surface.

Regressions are made for data outlined from the code. For this purpose the statistical code SPSS is used. For maximum flow depth along the centreline of the channel the final equation outlined from SPSS was:

$$\frac{h_{\max(CL)}}{h_0} = 1.16 \frac{(F_r)^{0.503} * \left(\frac{P_l}{h_0}\right)^{0.008} * \left(\frac{P_{th}}{h_0}\right)^{0.317}}{\left(\frac{B}{h_0}\right)^{0.009} * (S)^{0.131} * (Z)^{0.046}} \tag{14}$$

From the above equation it is clear that the aspect ratio and the pier length had no effect on the maximum flow depth along the centreline of the channel as is clear in Figures 13 and 16 as well, and Equation (14) can be reduced to:

$$\frac{h_{\max(CL)}}{h_0} = 1.16 \frac{(F_r)^{0.503} * \left(\frac{P_{th}}{h_0}\right)^{0.317}}{(S)^{0.131} * (Z)^{0.046}} \tag{15}$$

For maximum flow depth along the wall of the channel, the outline equation from regression of data is as below:

$$\frac{h_{\max(wall)}}{h_0} = 0.242 \frac{(F_r)^{0.534} * \left(\frac{P_l}{h_0}\right)^{0.131} * \left(\frac{P_{th}}{h_0}\right)^{0.148}}{\left(\frac{B}{h_0}\right)^{0.147} * (S)^{0.281} * (Z)^{0.086}} \tag{16}$$

It is clear from the above equations in the figures 18 to 22 as well that all the aforementioned factors affect the maximum flow depth along the wall of the channel, and that the side walls slope of the channel has less effect than the other parameters.

5 Conclusions

In the present investigation the impact of variations in aspect ratio, bed and side wall slopes of the channel, pier length and thickness on maximum flow depth, both at the centreline and the wall of the channel were conducted. The results demonstrate that CFD code is a suitable tool for simulating flow in high velocity channels with a single bridge pier at full scale. The simulation of full scale flow environments is possible using numerical modelling in this way,

without the cost of producing physical models for a prototype, and the study has demonstrated that such large scale simulations are possible by using parallel computation with HPC.

The methodology used here relies on validation of the model for a similar flow case using physical experiment data before running the parametric investigations numerically. The study confirmed that the flow situation studied here can be considered symmetrical along the centreline of the channel, in order to save computational space and time, without loss of accuracy. It was also demonstrated that the $k-$ turbulence model is suitable for use in such situations involving straight high velocity channels with a single bridge pier; this is consistent with the results of (Lai, Weber & Patel, 2003).

The results show that the maximum flow depth along the centreline of the channel is not affected by the variations of the aspect ratio and pier length, but is directly proportional to variations in the bed slope of the channel, discharge capacity, and pier thickness. The impact of variations in the side wall slope of the channel is inversely proportional to changes in the maximum flow depth at the centerline of the channel. Regression analysis has been carried out for data obtained from the numerical simulations. The maximum flow depth along the centerline of the channel is shown to be unaffected by the different values of aspect ratio and pier length.

Both pier length and thickness are directly proportional to changes in the maximum flow depth along the wall of the channel, while the impact of variations in aspect ratio, bed and side wall slopes of the channel, is inversely proportional to changes in the maximum flow depth at the centreline of the channel. Further, it has been shown using regression analysis that the value of the maximum flow depth along the wall of the channel was less affected by the side walls slope of the channel than by the other factors.

Acknowledgments

This work was conducted in the coastal and ocean engineering research group (COERG) and using the high performance computer, HPC, cluster at the School of Marine Science and Engineering, Plymouth University. Funding was provided by the Ministry of Higher Education and Scientific Research, Iraqi government.

REFERENCES

ANSYS, I. (2009) *ANSYS-CFX, version 12.0,* . (Version 14) [Computer Program]. Canonsburg, PA. : Available

Berger, R. & Stockstill, R. (1995) 'Finite-element model for high-velocity channels'. *J. Hydr. Eng.*, 121 (10). pp 710-716.

Chiu, C. L. (1988) 'Entropy and 2-D velocity distribution in open channels'. *J. Hydr. Eng.*, 114 (7). pp 738-756.

French, R. H. (1985) *Open Channel Hydraulics*. 2nd Printing 1987 Singapore: McGraw-Hill Book New Yourk.

Hirt, C. W. & Nichols, B. D. (1981) 'Volume of fluid (VOF) method for the dynamics of free boundaries'. *Journal of computational physics*, 39 (1). pp 201-225.

Hos, C. & Kullman, L. (2007) 'A numerical study on the free-surface channel flow over a bottom obstacle'. *Journal of Hydraulic Research*, 42 (3). pp 263–272.

Ippen, A. T. (1951) 'High-Velocity Flow in Open Channels: A Symposium: Mechanics of Supercritical Flow'. *Transactions of the American Society of Civil Engineers*, 116 (1). pp 268-295.

Ippen, A. T. & Dawson, J. H. (1951) 'High-Velocity Flow in Open Channels: A Symposium: Design of Channel Contractions'. *Transactions of the American Society of Civil Engineers*, 116 (1). pp 326346.

Kallaka, T. & Wang, C. J. (2011) 'Efficient Numerical Model for Studying Bridge Pier Collapse in Floods'. World Acad Sci Eng Technol, 60 pp 1011-1016.

Knapp, R. T. (1951) 'High-Velocity Flow in Open Channels: A Symposium: Design of Channel Curves for Supercritical Flow'. Transactions of the American Society of Civil Engineers, 116 (1). pp 296-325.

Lai, Y. G. (2010) ' Two-Dimensional Depth Averaged Flow Modelling with an Unstructured Hybrid Mesh. '. J. Hydr. Eng ASCE. , 136 (1). pp 12-23.

Lai, Y. G. & Greimann, B. P. (2010) 'Predicting contraction scour with a two-dimensional depthaveraged model'. *Journal of Hydraulic Research*, 48 (3). pp 383-387.

Lai, Y. G., Weber, L. J. & Patel, V. C. (2003) 'Nonhydrostatic three-dimensional model for hydraulic flow simulation. I: Formulation and verification'. *J. Hydr. Eng.*, 129 (3). pp 196-205.

Marriott, M. J. & Jayaratne, R. (2010) 'Hydraulic roughness–links between Manning's coefficient, Nikuradse's equivalent sand roughness and bed grain size', *Nikuradse's equivalent sand roughness and bed grain size'Proceedings of Advances in Computing and Technology,(AC&T) The School of Computing and Technology 5th Annual Conference, University of East London*. University of East London, School of Computing, Information Technology and Engineering, pp. 27-32.

MMSWM (1976) ' Manual of the management of storm water in mancipal area for -Iraq '.[in first edition edn. (Accessed:MMSWM

Rouse, H., Bhoota, B. & Hsu, E.-Y. (1951) 'High-Velocity Flow in Open Channels: A Symposium: Design of Channel Expansion'. *Transactions of the American Society of Civil Engineers*, 116 (1). pp 347-363.

Stockstill, R. L. (1996) *A Two-Dimensional Free-Surface Flow Model for Trapezoidal High-Velocity Channels.* DTIC Document. Available.

Stockstill, R. L. B., R. C. and Nece, R. E. (1997) 'Two-dimensional flow model for trapezoidal highvelocity channels'. *J. Hydr. Eng. ASCE*, 123 (10). pp 844-852.